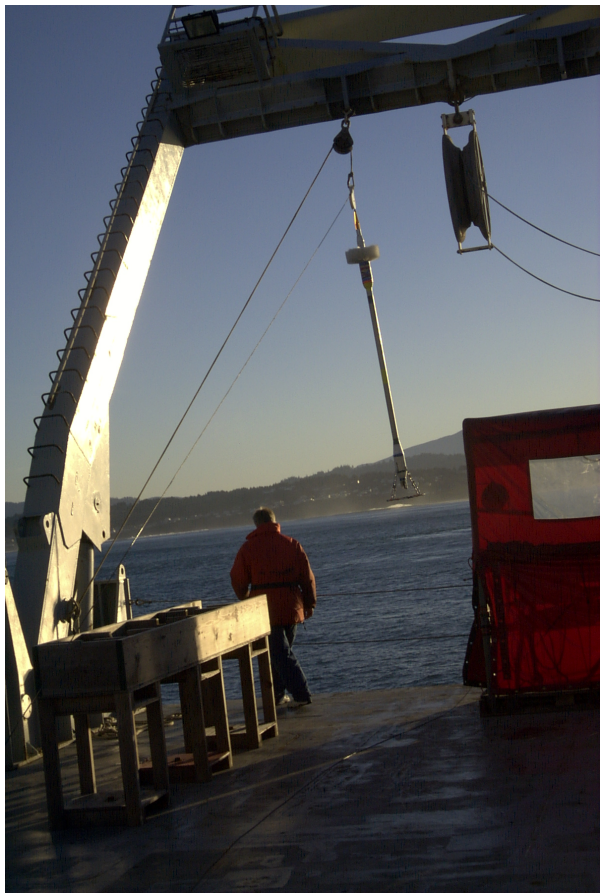
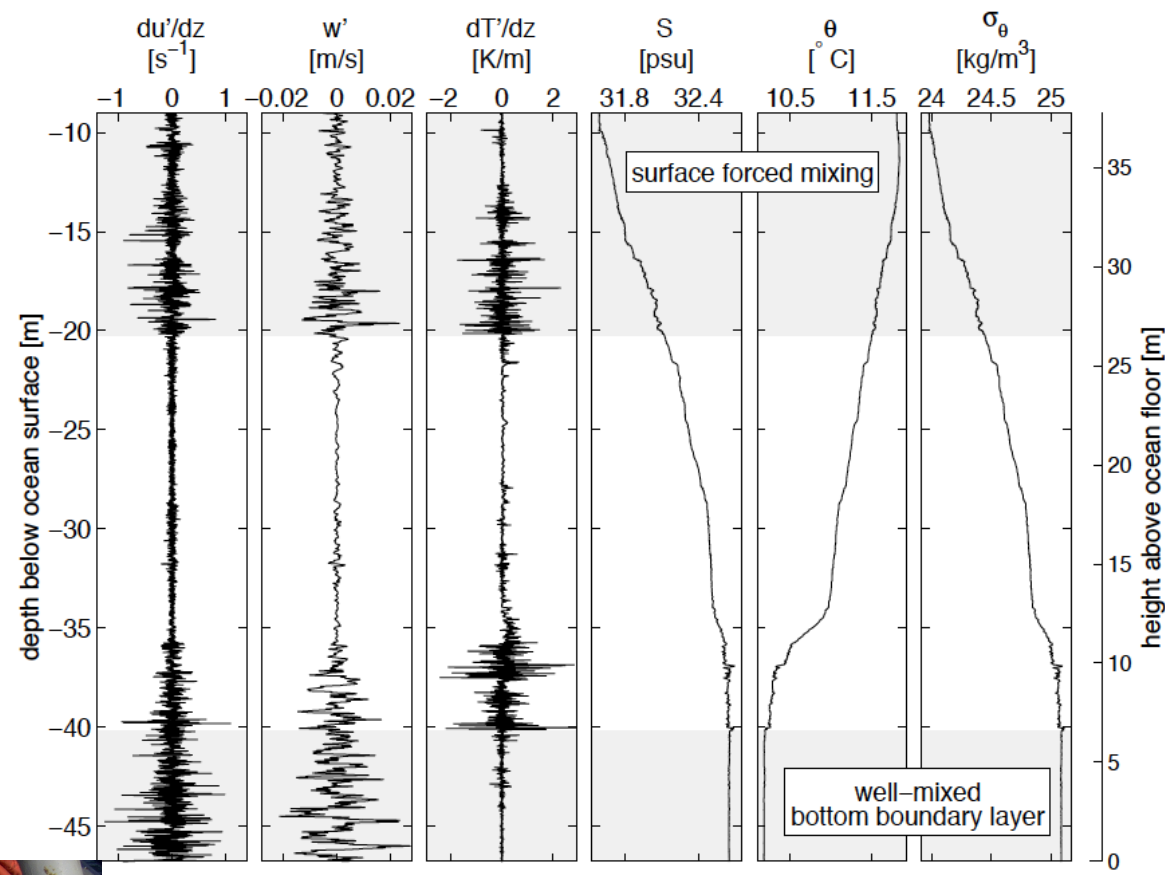


## Buoyancy effects

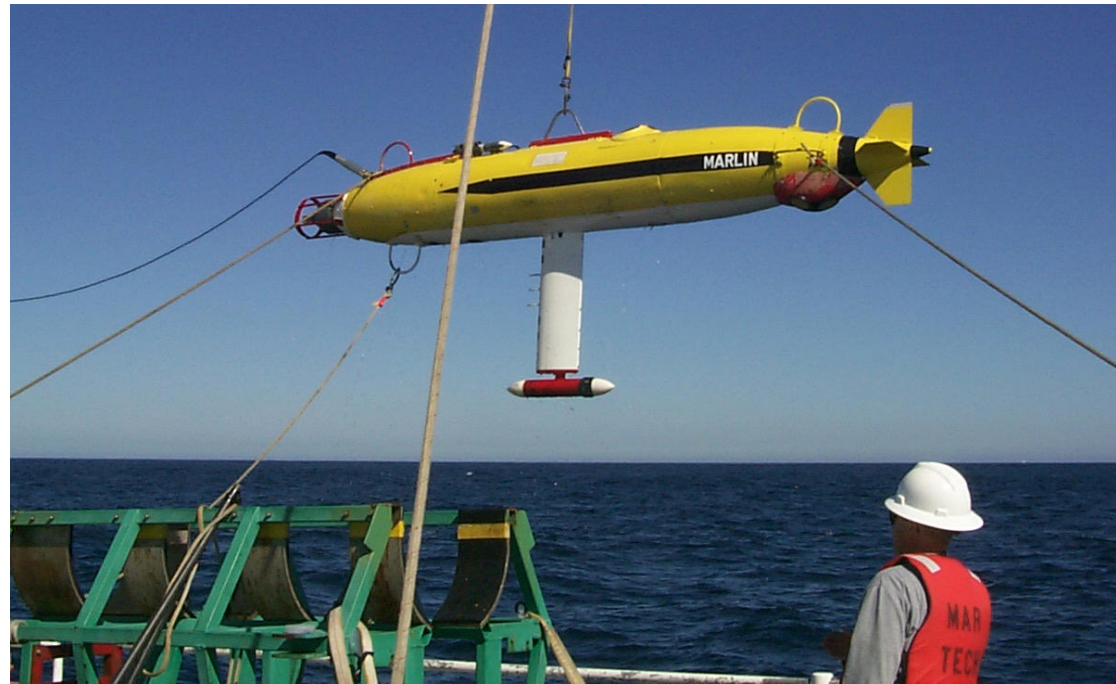
<https://youtu.be/FYX1Tusmhd4>





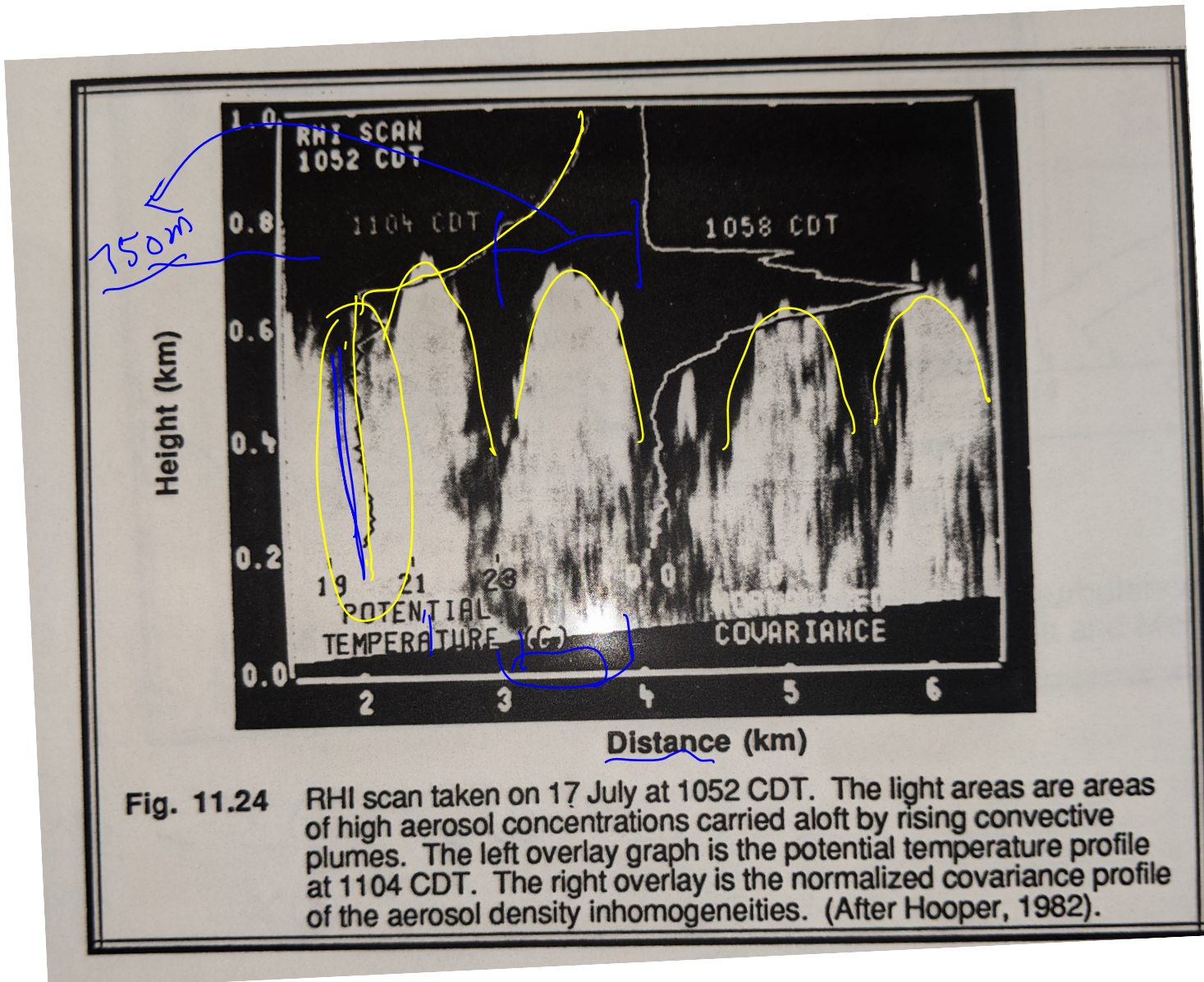


## Research Platform FLIP

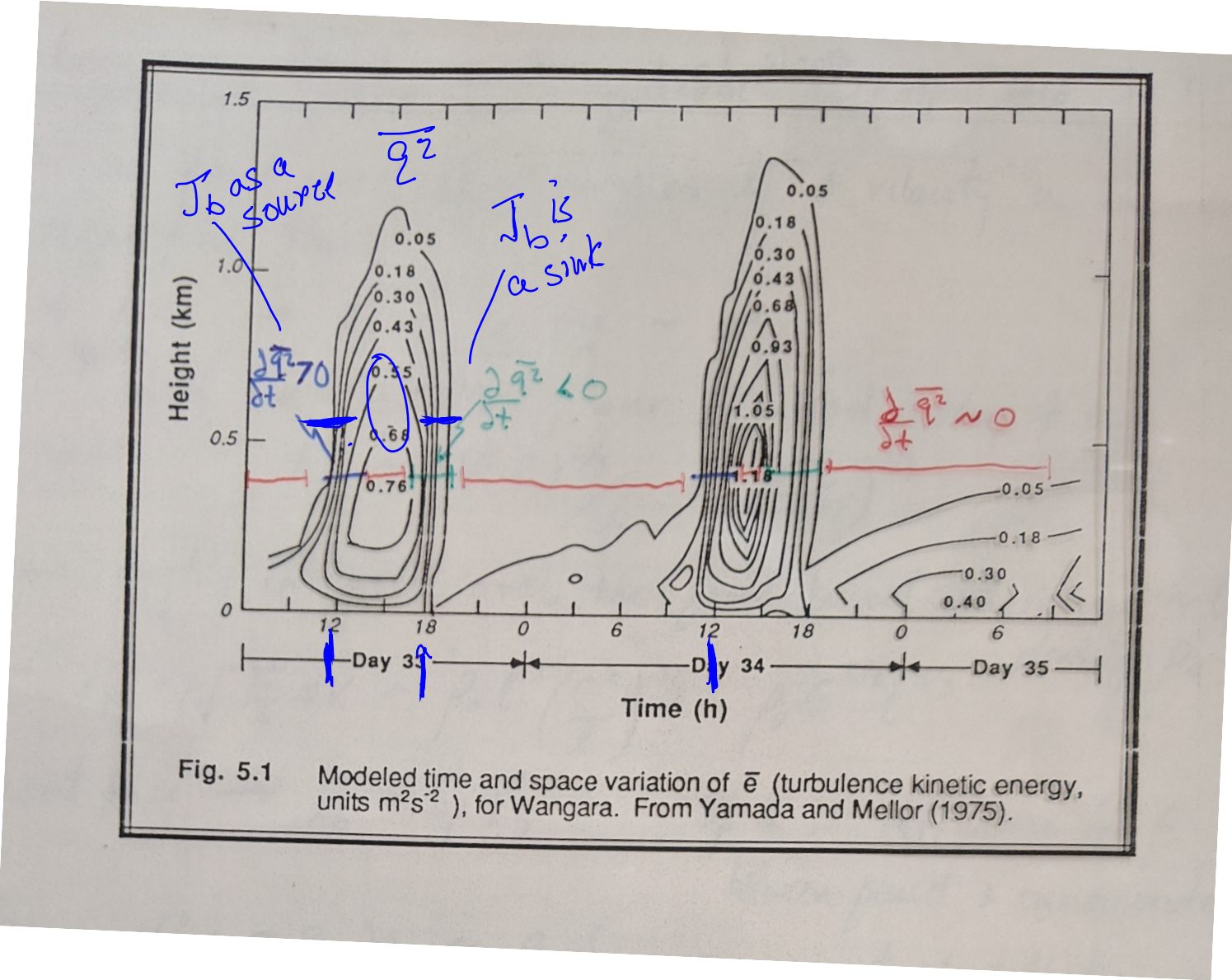


Buoyancy flux ( $B$  or  $J_b$ ) as a source of TKE

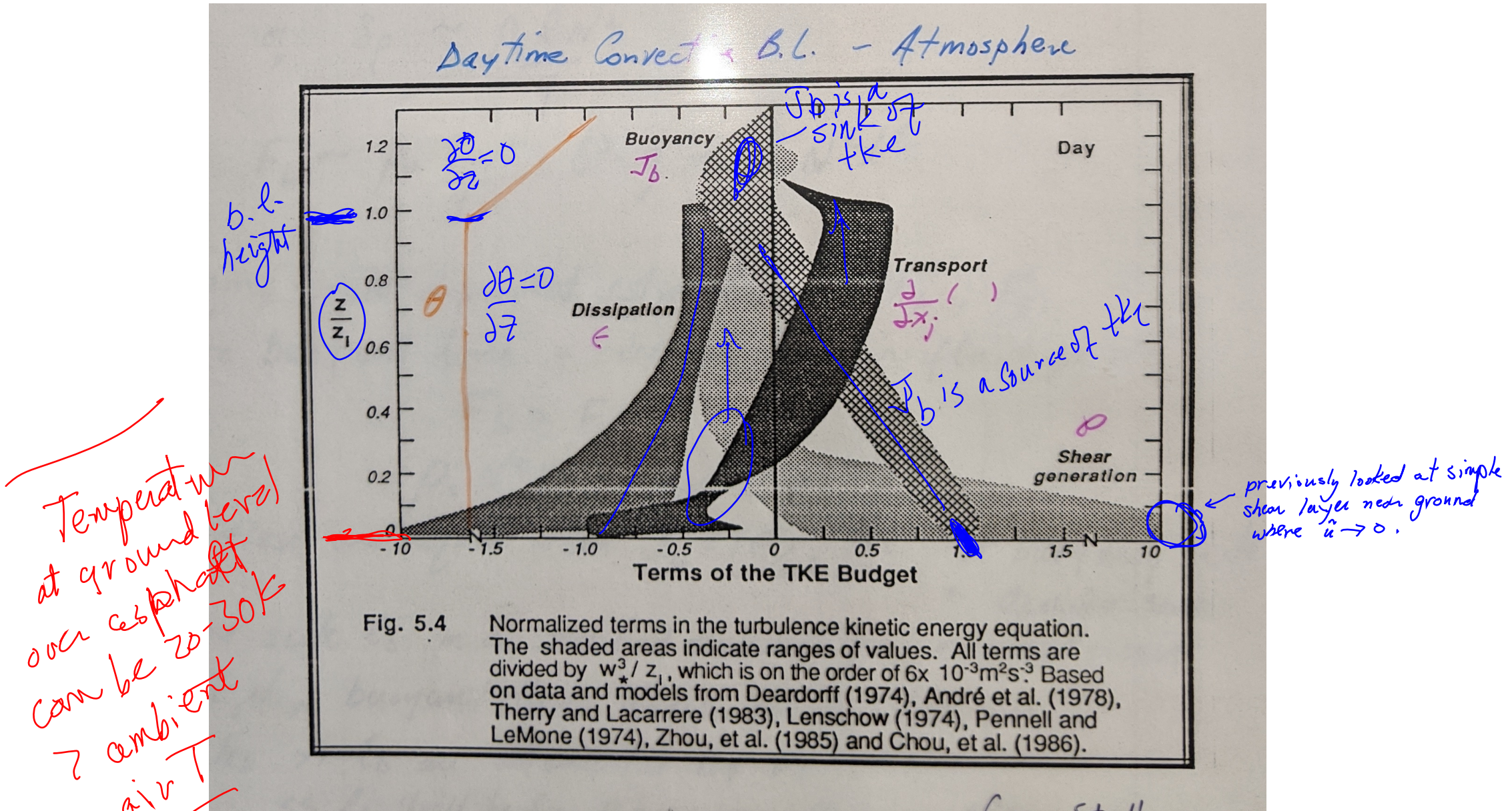
## Daytime Convection – Atmospheric Boundary Layer



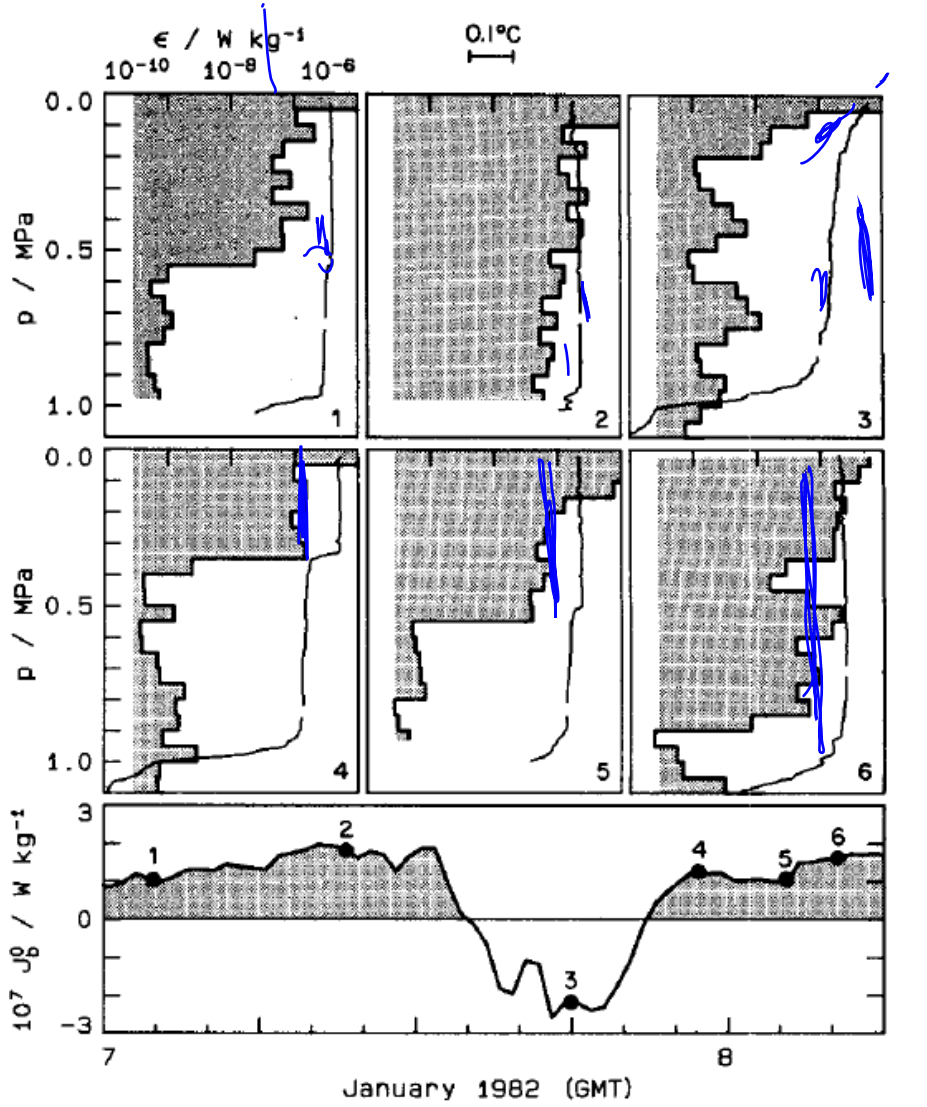
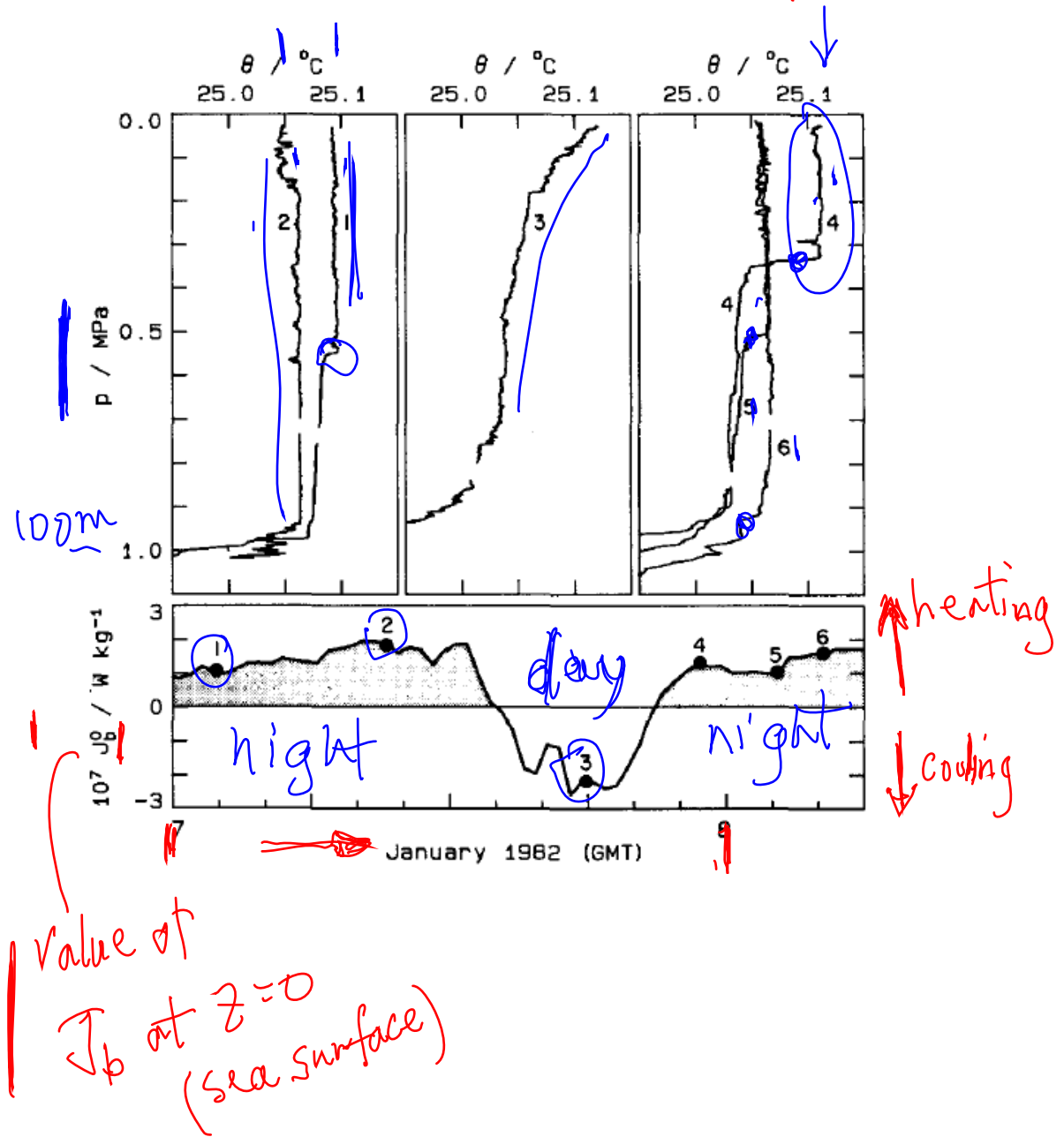
## Daytime Convection – Atmospheric Boundary Layer



# Daytime Convection – Atmospheric Boundary Layer



$$10^{-7} \text{ N/kg} = 10^{-7} \text{ m}^2/\text{s}^3$$



Shay and Gregg 1986

$$\psi = \epsilon / J_b^0$$

bottom of trop-

During highly convective conditions, such that buoyancy flux is the dominant TKE source term

important. Under these conditions, the characteristic length, velocity, and time scales are

$$\rightarrow l_* = D \quad [m] \quad (7)$$

$$\rightarrow W_* = (D J_b^0)^{1/3} \quad [m s^{-1}] \quad (8)$$

$$\rightarrow T_* = \frac{D}{W_*} \quad [s]. \quad (9)$$

Using the convective mixed layer scales, the dimensionless form of the viscous dissipation rate becomes

$$\Psi = \frac{\epsilon D}{W_*^3} = \frac{\epsilon}{J_b^0}. \quad (10)$$

$$\Psi(z) = \frac{\epsilon(z)}{J_b^0}$$

$$\epsilon \sim J_b^0$$

$$\epsilon \sim u^3/l$$

$$W_* \sim (D J_b^0)^{1/3}$$

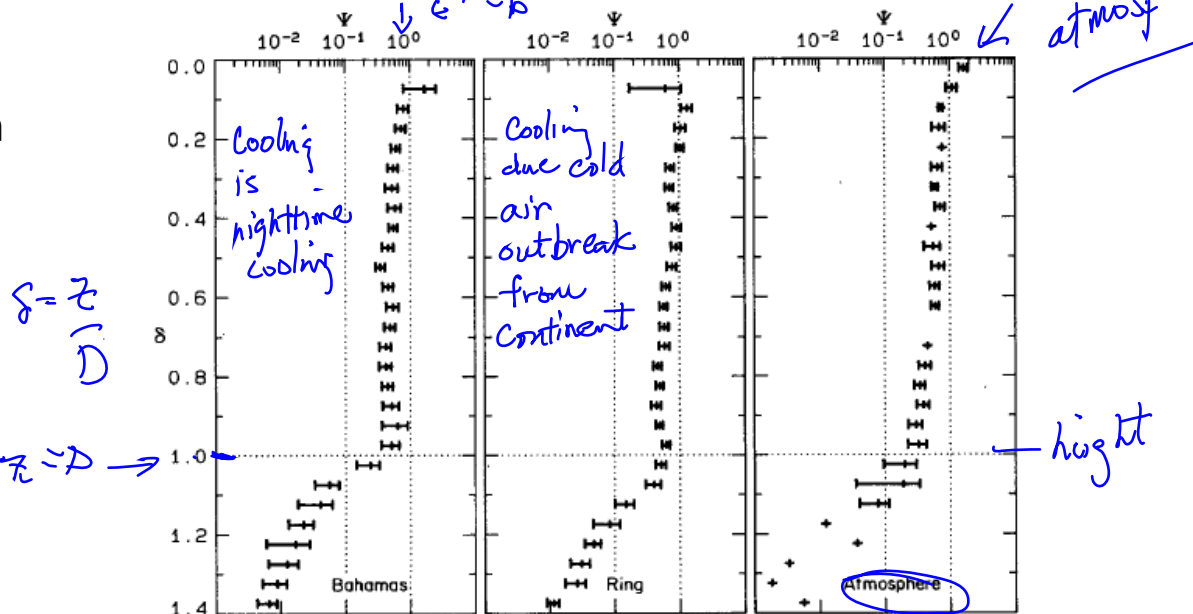


FIG. 17. Profiles of viscous dissipation rate nondimensionalized using convective mixed layer scaling. The atmospheric data are from Caughey and Palmer (1979) and have been ensemble averaged to appear on the same  $\delta$  grid as the oceanic data. The error bars are 95% confidence intervals calculated using the bootstrap method. The mean values of  $\Psi$  in the mixed layers ( $0 < \delta < 1$ ) are 0.61 (Bahamas), 0.72 (ring) and 0.64 (atmosphere).

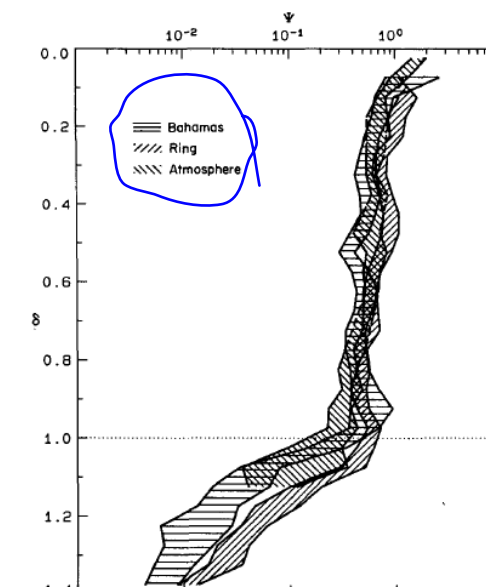


FIG. 18. Envelopes of the 95% confidence intervals overlaid to show that, at most depths in the mixed layer, the three datasets are statistically the same.

# vertical structure of the geophysical convective boundary layers

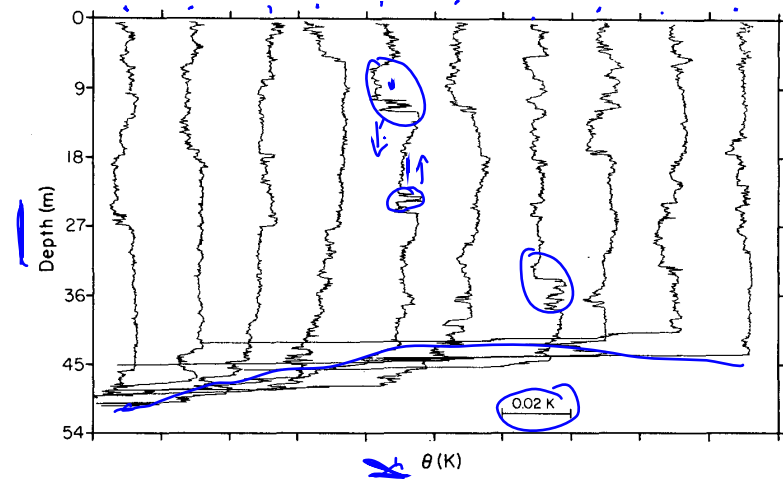


FIG. 1. A typical set of 10 consecutive vertical potential temperature ( $\theta$ ) profiles during nighttime convective conditions. The profiles were taken between local time 0134 and 0239 and the horizontal spacing between profiles is about 900 m. Each profile was referenced to the temperature in the mixed layer by subtracting the average potential temperature in the mixed layer ( $-D < z < 2L$ ). Profiles are offset by 0.02 K. The potential temperature  $\theta$  is the temperature the fluid parcel would have if it was expanded or compressed adiabatically (i.e., without thermal contact with the surrounding fluid) from its existing pressure and temperature to a standard reference pressure. This removes the influence of pressure on temperature and is useful when comparing fluid parcels at different depths and when considering vertical motions of fluid parcels. In an adiabatic layer  $\theta$  is constant with depth (i.e., a vertical line) and in a superadiabatic layer the vertical derivative of  $\theta$ ,  $\partial\theta/\partial z$ , is negative.

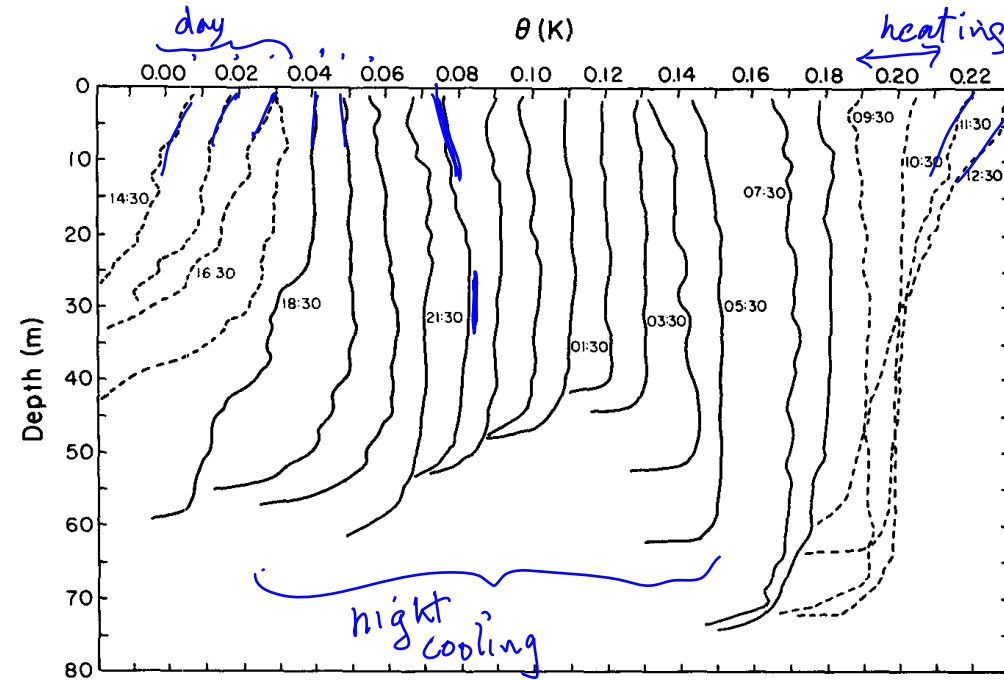


FIG. 2. A sequence of referenced and hourly averaged  $\theta$  profiles throughout one diurnal cycle, starting at 1430 local time and ending the following day at 1230. Solid lines are nighttime profiles and broken lines are daytime profiles; profiles are offset by 0.01 K. From this sequence it is observed that the small superadiabatic potential temperature gradient, in the upper part of the profiles, is a persistent feature throughout the night (but away from transition periods). The transition time from  $\partial\theta/\partial z > 0$  during daytime, to  $\partial\theta/\partial z < 0$  during nighttime (and vice versa) is on the order of 2 hours. The 0630 profile is missing due to instrumentation problems.

Rayleigh-Benard Instability  
denser fluid over lighter fluid  
gravity will pull the cooler fluid &  
→  $\rho'g$   
Gravitational force is opposed by viscous damping on the fluid parcel  
The balance of gravity & viscous forces is represented by

$$Ra = \frac{g\alpha(T_L - T_u)L^3}{\nu\gamma}$$

$T_u$  - upper T  
 $T_L$  - lower T  
 $L$  - vertical scale  
 $\alpha$  - thermal exp. coeff.  
 $\gamma$  - thermal diff.

so strictly this applies to 2 flat plates, with bottom heated and defines the  $\delta T = T_L - T_u$  or  $L$  reqd for instability

and formation of regular cells. that hexagonal under perfect conditions are similar to cumulus clouds at top of mixed layer during daytime convection in ABL.

Anis & Moum 1992

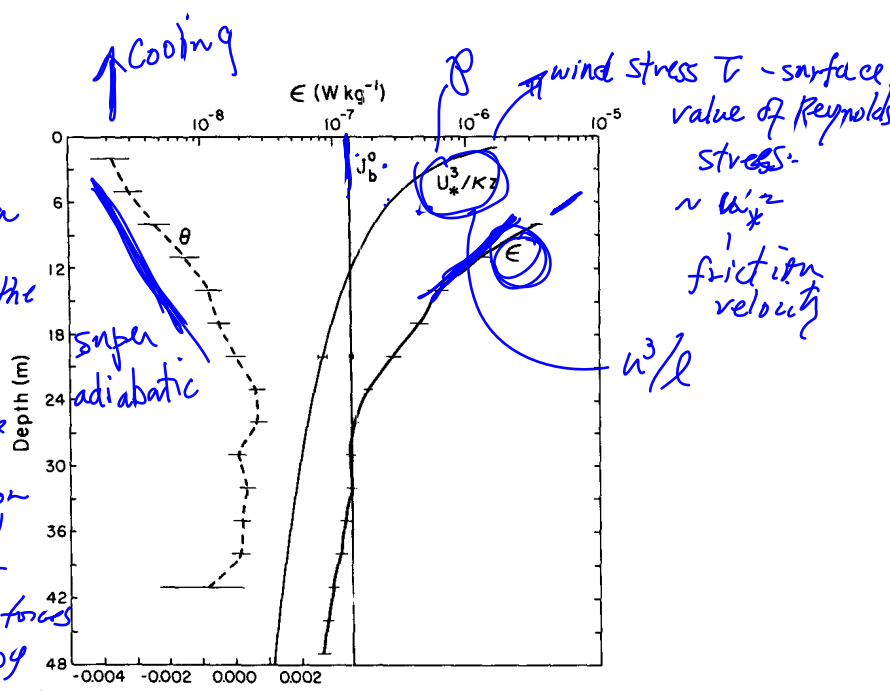
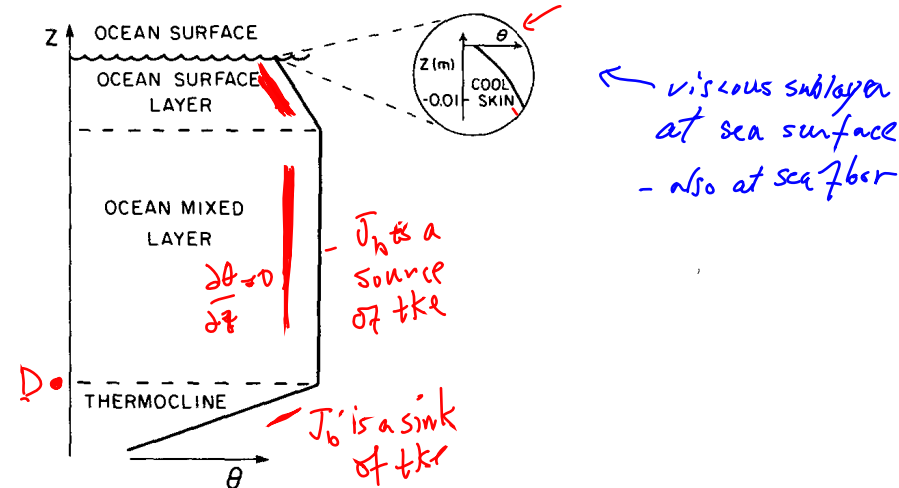


FIG. 5. Referenced and averaged  $\theta$  profile and averaged  $\epsilon(z)$  profile for night 3. The production terms of TKE by surface winds ( $u_*^3/kz$ ) and by surface buoyancy flux ( $J_b^0$ ) are plotted also. Although  $\epsilon(z)$  is reasonably constant within the mixed layer, it is not so in the surface layer.  $\epsilon(z)$  increases toward the surface at a greater rate than each of the sum of the production terms ( $u_*^3/kz$  and  $J_b^0$ ).  $\epsilon(z)$  values from depths shallower than 6.5 m were omitted due to possible contamination by the ship's wake. Error bars are 95% bootstrap confidence limits.

critical Ra = 1700  
for gravity to exceed viscous damping + instability - for simple case

### OCEANIC CONVECTIVE BOUNDARY LAYER



### ATMOSPHERIC CONVECTIVE BOUNDARY LAYER

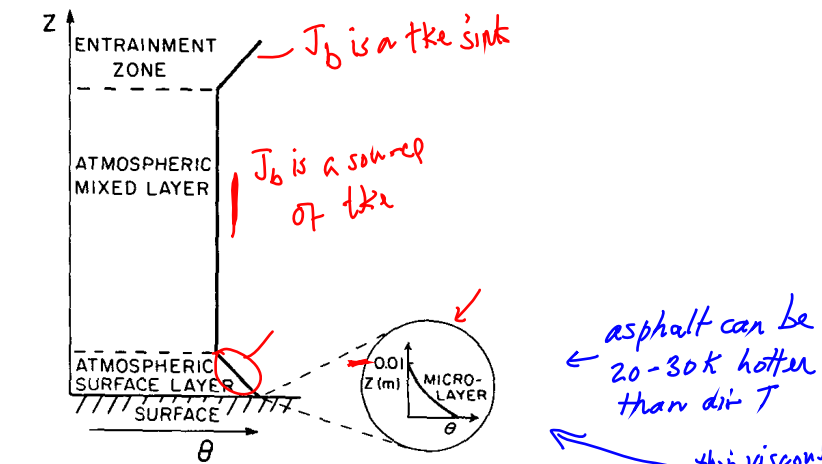


FIG. 6. Schematic showing the mean potential temperature structure of the oceanic and atmospheric CBLs. Table 2 presents a summary of the main characteristics of each layer.

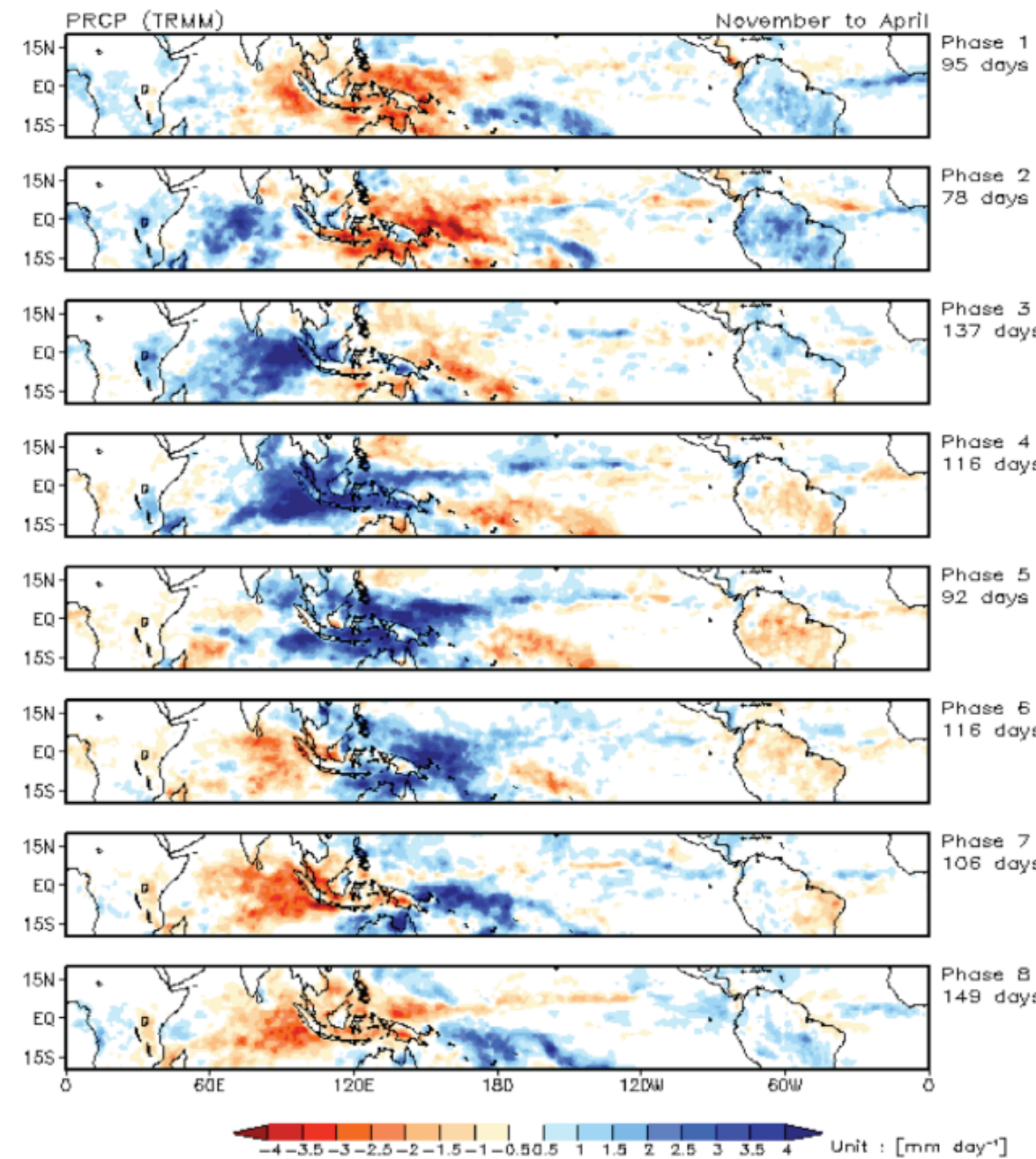
Buoyancy flux ( $B$  or  $J_b$ ) as a sink of TKE

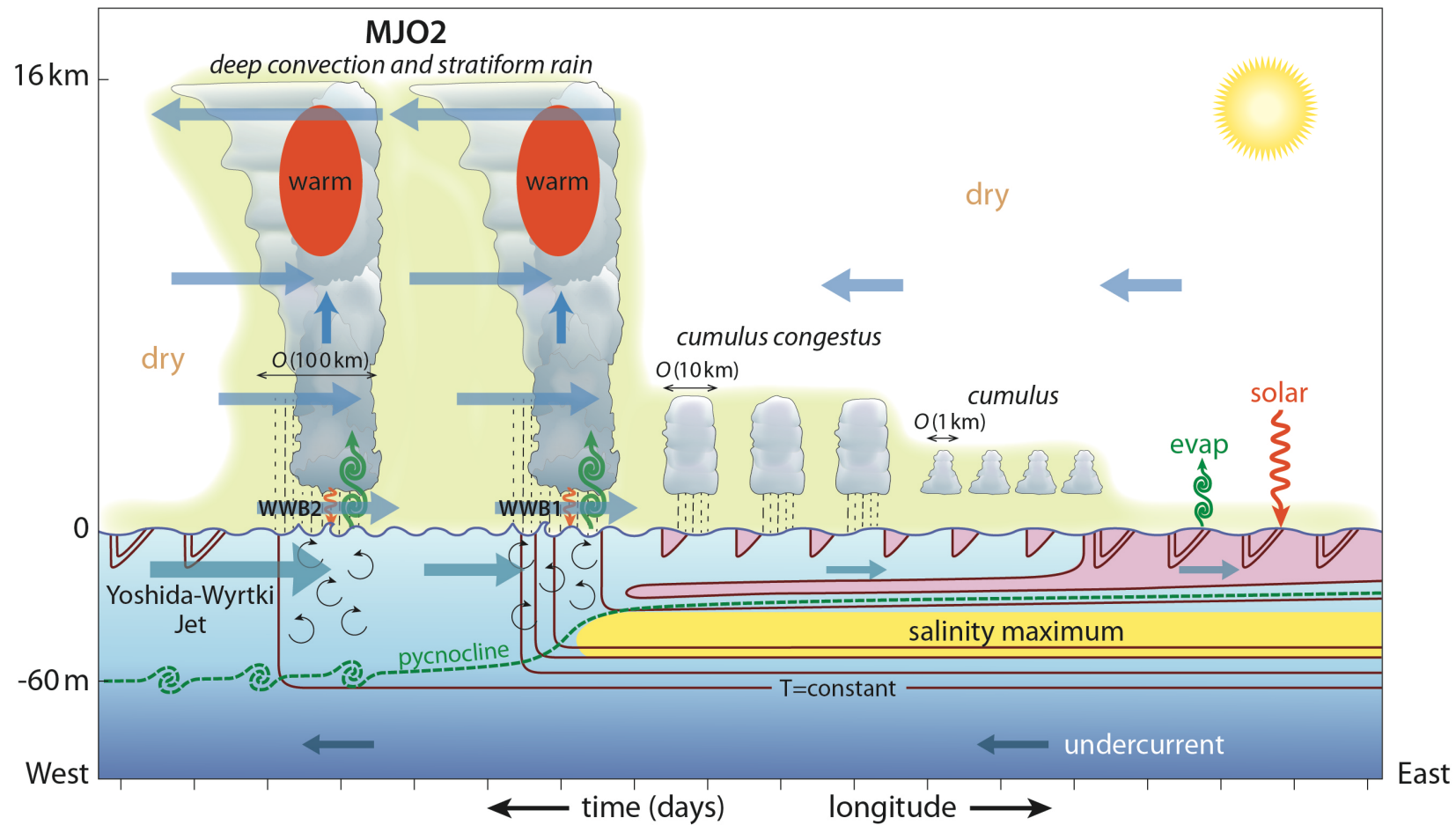
But 1<sup>st</sup> go back to whiteboard  
and define a buoyancy length scale

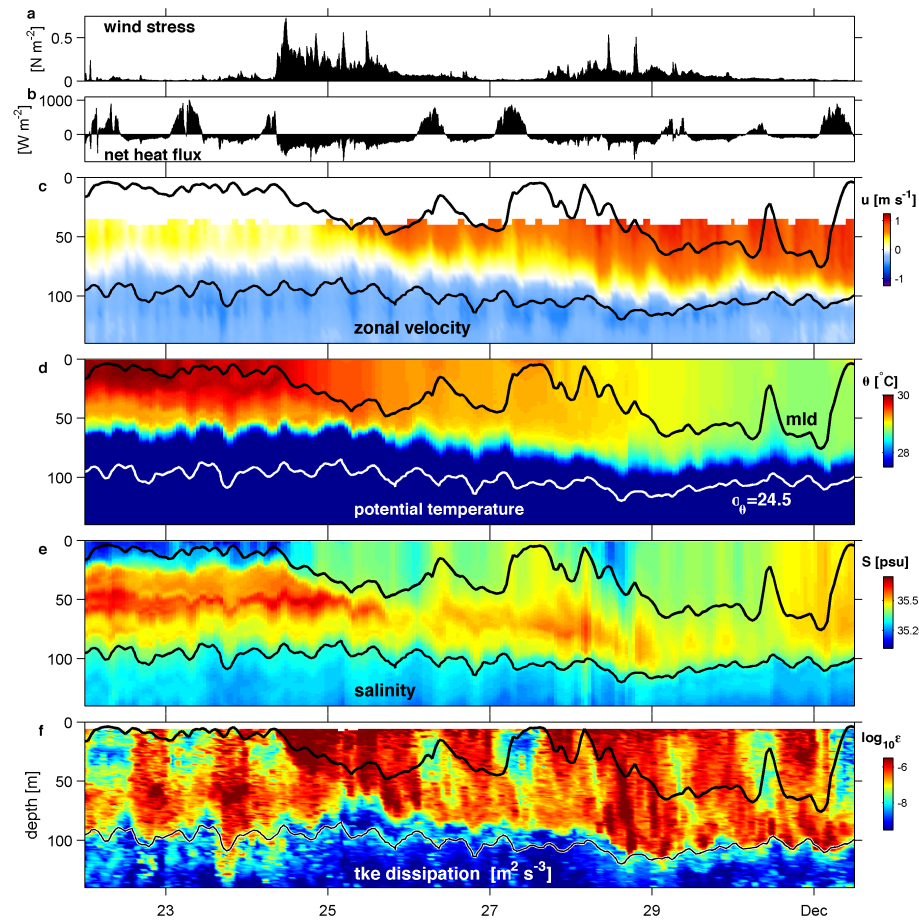
$$l_b \text{ or } h_0 = (\epsilon/N^3)^{1/2}$$

$\uparrow$        $\uparrow$   
buoyancy      Ozmidov

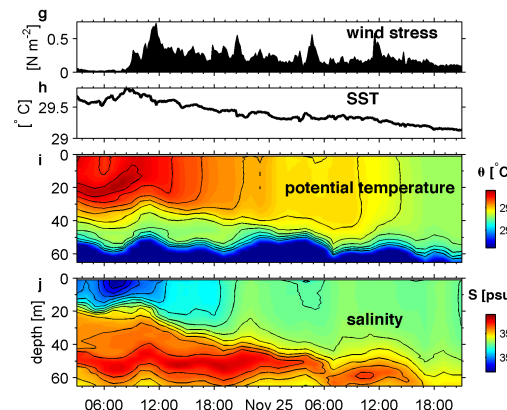
### MJO Life cycle composite







focus on the  
barrier layer

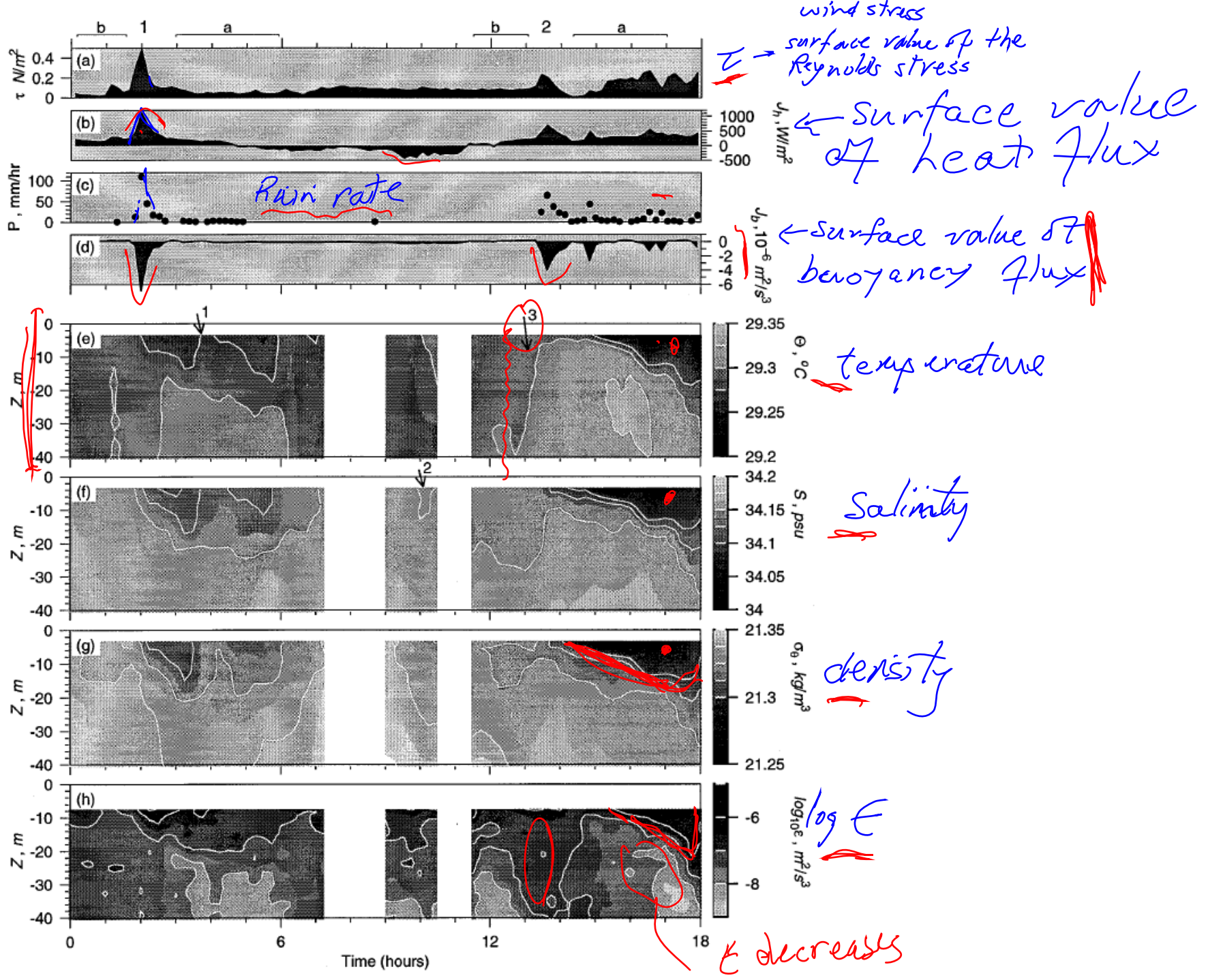


# **Decay of Turbulence in the Upper Ocean following Sudden Isolation from Surface Forcing**

## **3. Surface signature of squalls**

The term squall, or squall line, refers to a convective atmospheric structure that is organized in a linear fashion and is associated with a cold front, increased winds, and strong precipitation. Over the equatorial ocean, squall lines are common, accounting for up to 50% of annual rainfall (e.g., Zipser 1977). At the ocean surface, the passage of a squall is generally accompanied by

- a rapid increase in wind speed (up to 70 kt),
- a drop in air temperature ( $\sim 5^{\circ}\text{C}$ ),
- heavy rainfall (rain rates as high as 500 mm/h have been reported) (Houze 1977).



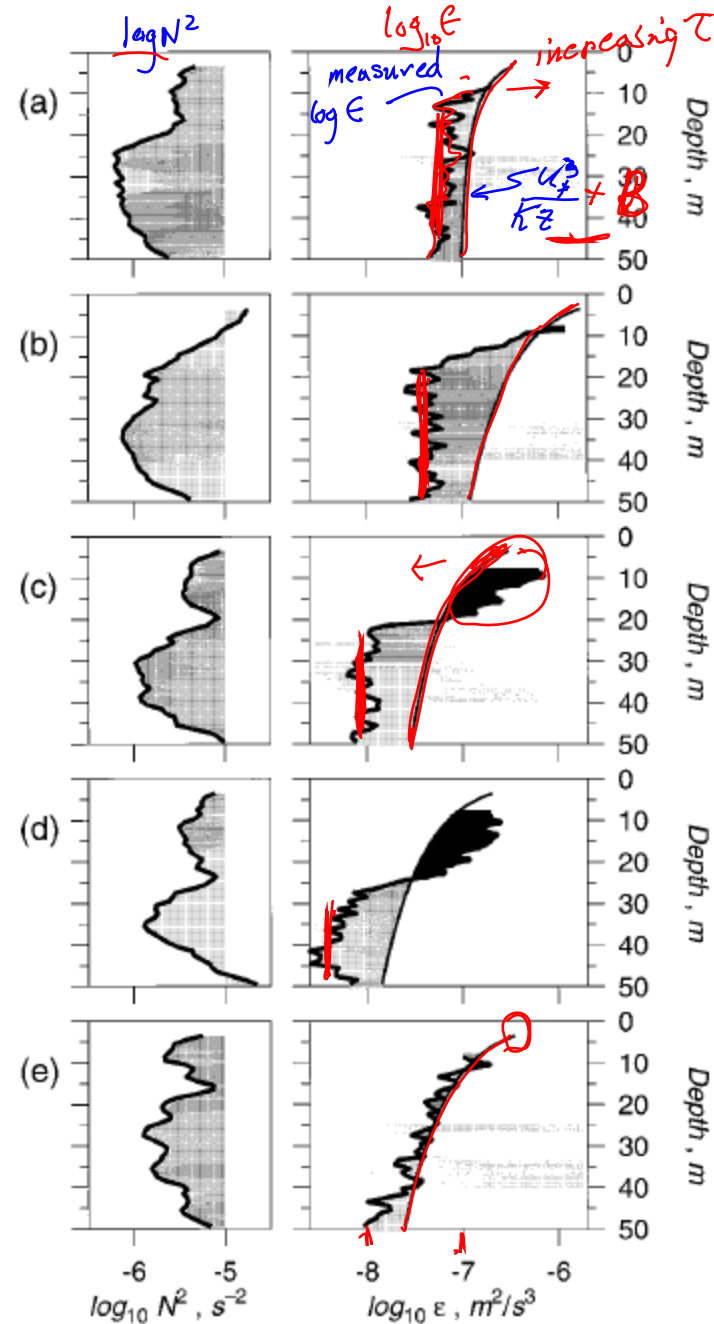
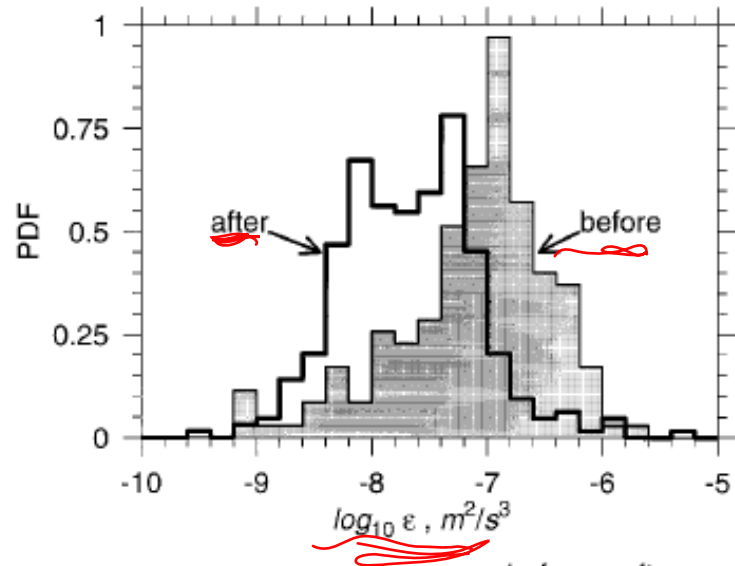


FIG. 2. Vertical profiles of  $N^2$  (left-hand frame) and  $\epsilon$  (right-hand frame), averaged over 10 consecutive profiles before (a;  $t = 0.2\text{--}1.6$  h), during (b;  $t = 1.6\text{--}3.0$  h) and after the passage of a squall (c, d, e;  $t = 3.0\text{--}4.4$  h,  $t = 4.4\text{--}5.9$  h,  $t = 5.9\text{--}7.3$  h, respectively). The squall is number 1, illustrated in Fig. 1. For comparison, the depth-dependent effects of combined surface buoyancy flux and wind stress are approximated by boundary layer similarity scaling  $\epsilon \sim u_*^3/\kappa z + 0.6J_b$ , in which  $u_*$  is the friction velocity,  $\kappa = 0.4$  is von Kármán's constant, and  $J_b$  is the surface buoyancy flux (Lombardo and Gregg 1989). The second term is included only when it is positive. Observed (theoretical) values are shown by the thick (thin) curve on the right-hand frame. Horizontal lines on the right-hand frames delineate the depth range over which the decay rate of  $\epsilon$  was evaluated.



	before	after
Median	-7.00	-7.66
Mean	-7.12	-7.67
Standard Deviation	0.66	0.59
Standard Error in Mean	0.05	0.03

FIG. 3. Probability distribution functions for  $\log_{10}\epsilon$  in the depth range 15–30 m before and after squall number 2. The “before” (“after”) case spans  $t = 11.5\text{--}13.0$  h ( $t = 15.9\text{--}17.0$  h). These intervals are intended to represent conditions prevailing when the squall arrived and during the ocean’s recovery and were chosen subjectively on the basis of meteorological data only.

$$\frac{d}{dt} \frac{3}{2} u^2 = -\varepsilon \quad (1)$$

$$\varepsilon = cu^3 / \ell \rightarrow \ell_b$$

$$\ell_b, \ell \rightarrow \ell = \left( \frac{\varepsilon}{N^3} \right)^{1/2}$$

$$\rightarrow \varepsilon = cu^2 N$$

solutions to (1)

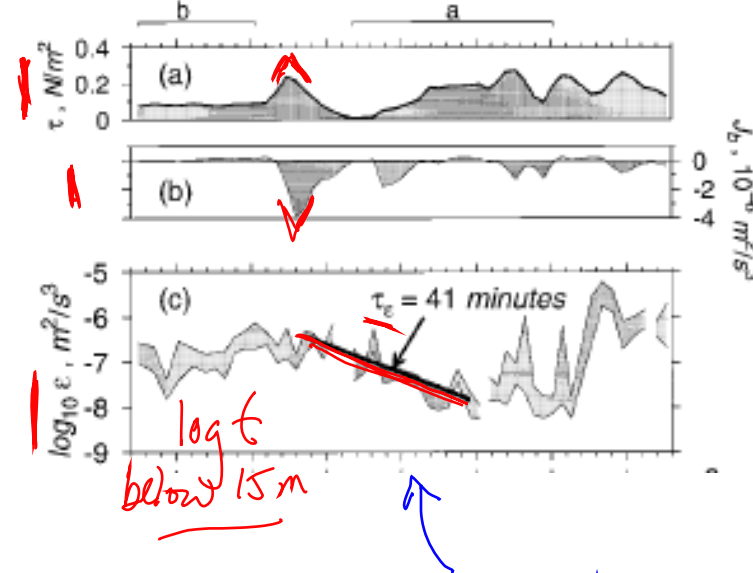
$$u \propto e^{-cNt}$$

$$\varepsilon \propto e^{-cNt}$$

decay of turbulence in  
a stratified fluid

→ much faster than in  
an unstratified fluid.

observed exponential decay  
of  $\varepsilon$  following rain squall

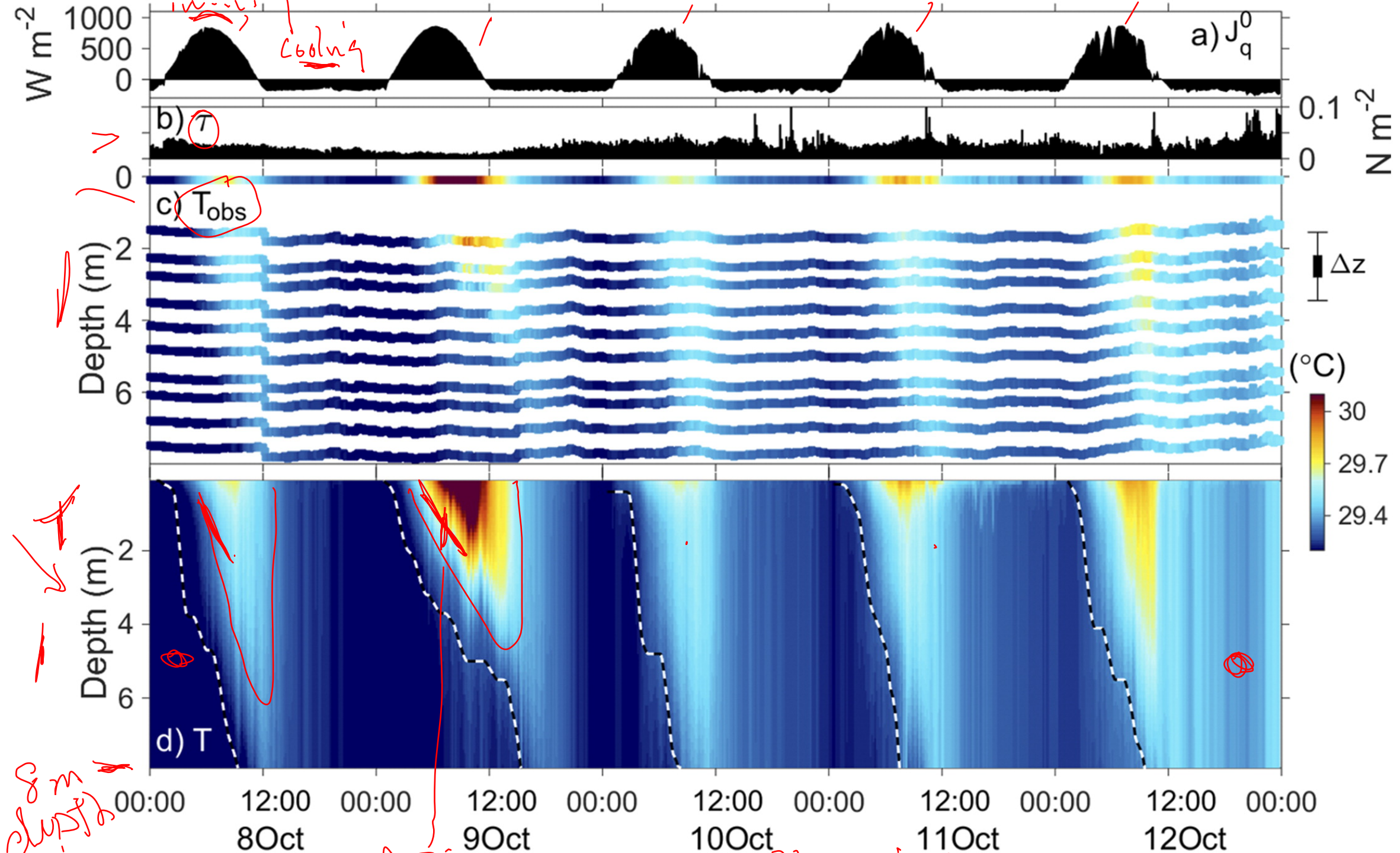


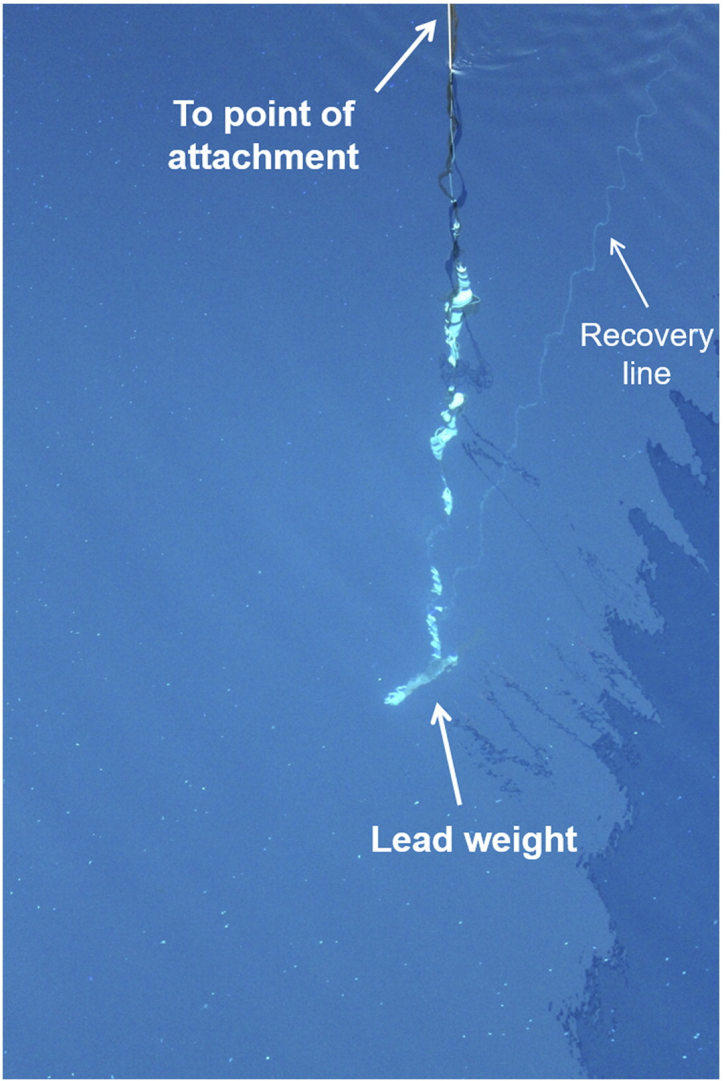
$\varepsilon$  decays by a  
factor 100 in  
40 minutes - roughly  $\sqrt[2]{T}$

## **Evolution of Turbulence in the Diurnal Warm Layer**

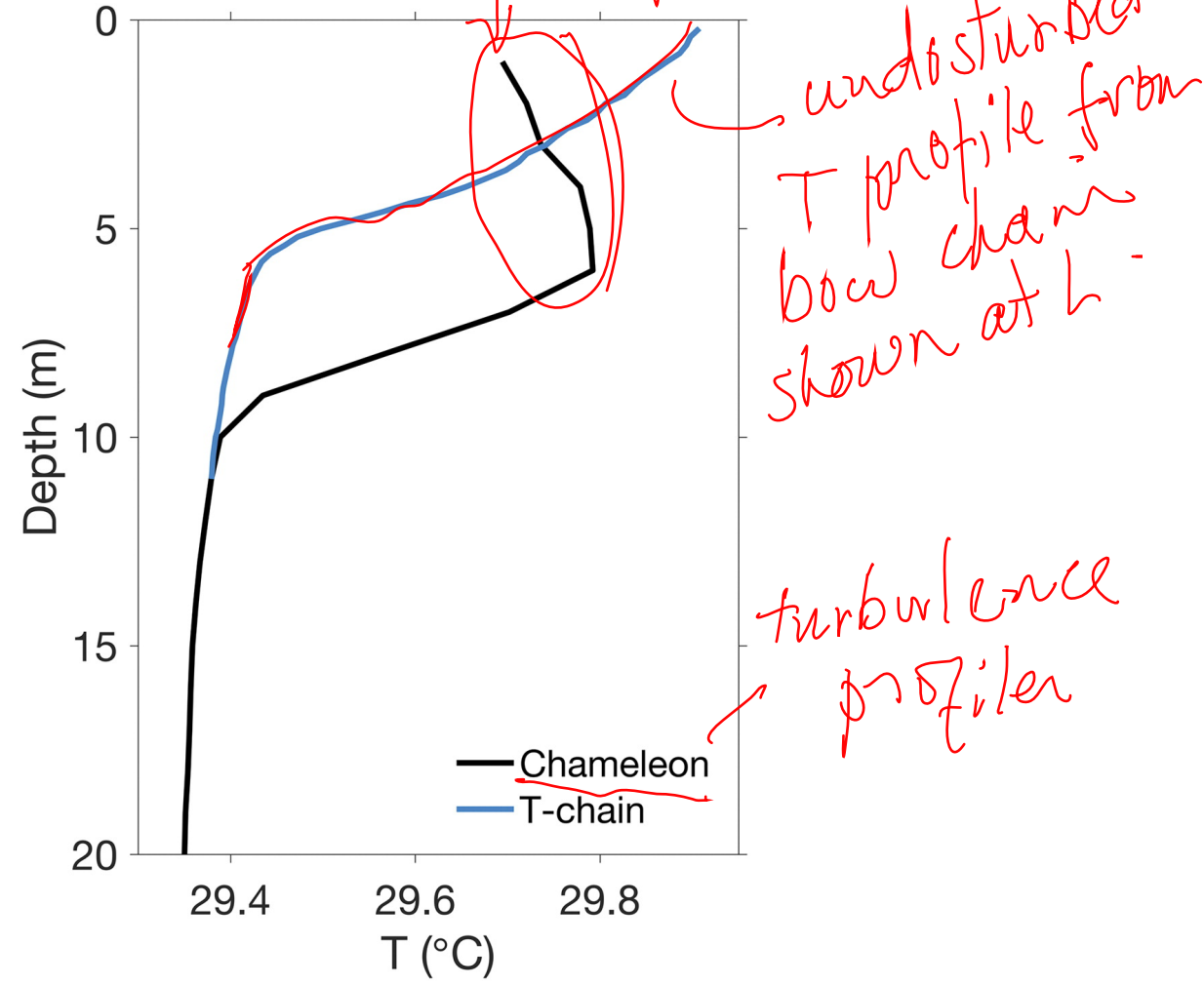
Aurélie J. Moulin, James N. Moum, and Emily L. Shroyer

<https://journals.ametsoc.org/doi/full/10.1175/JPO-D-17-0170.1>

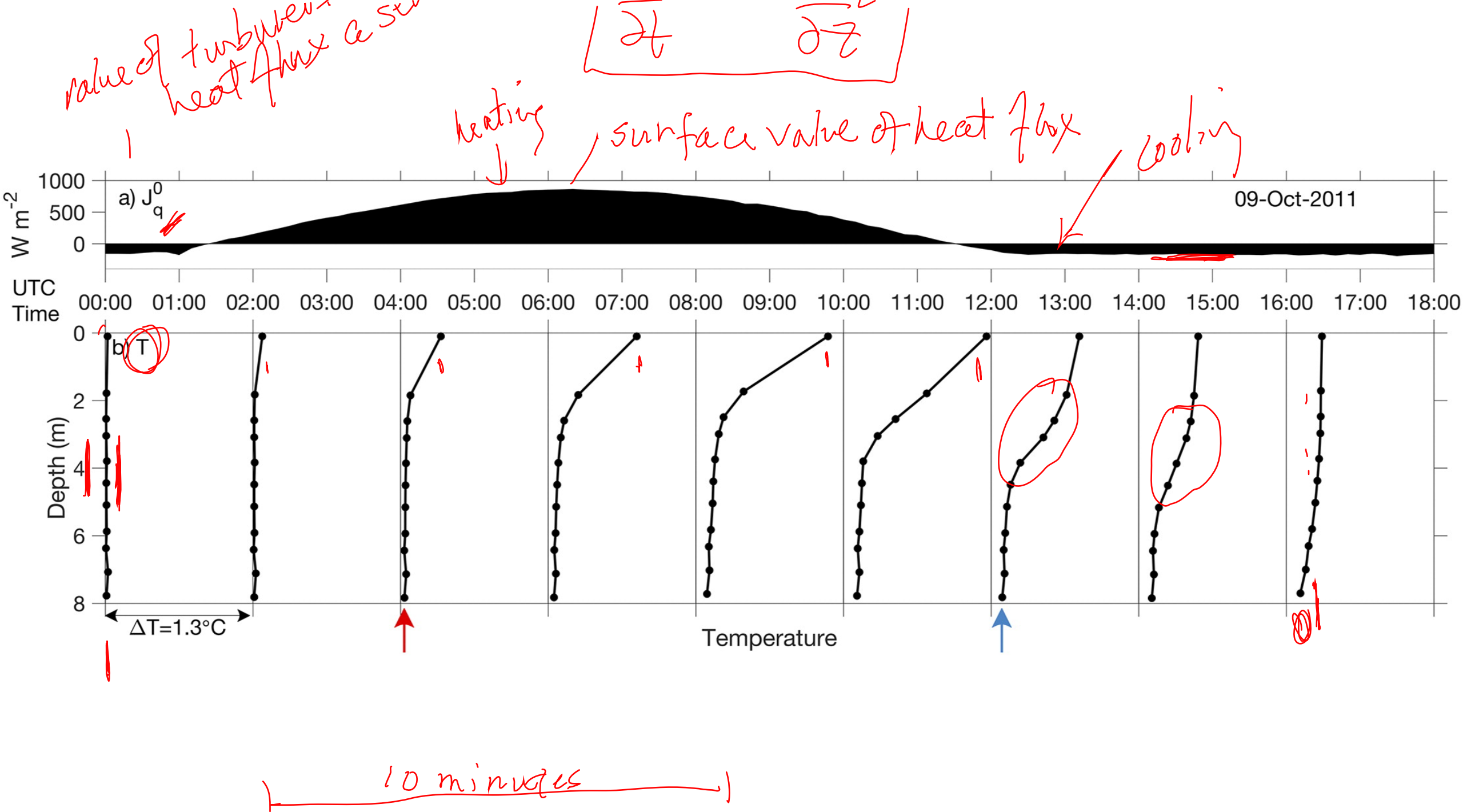


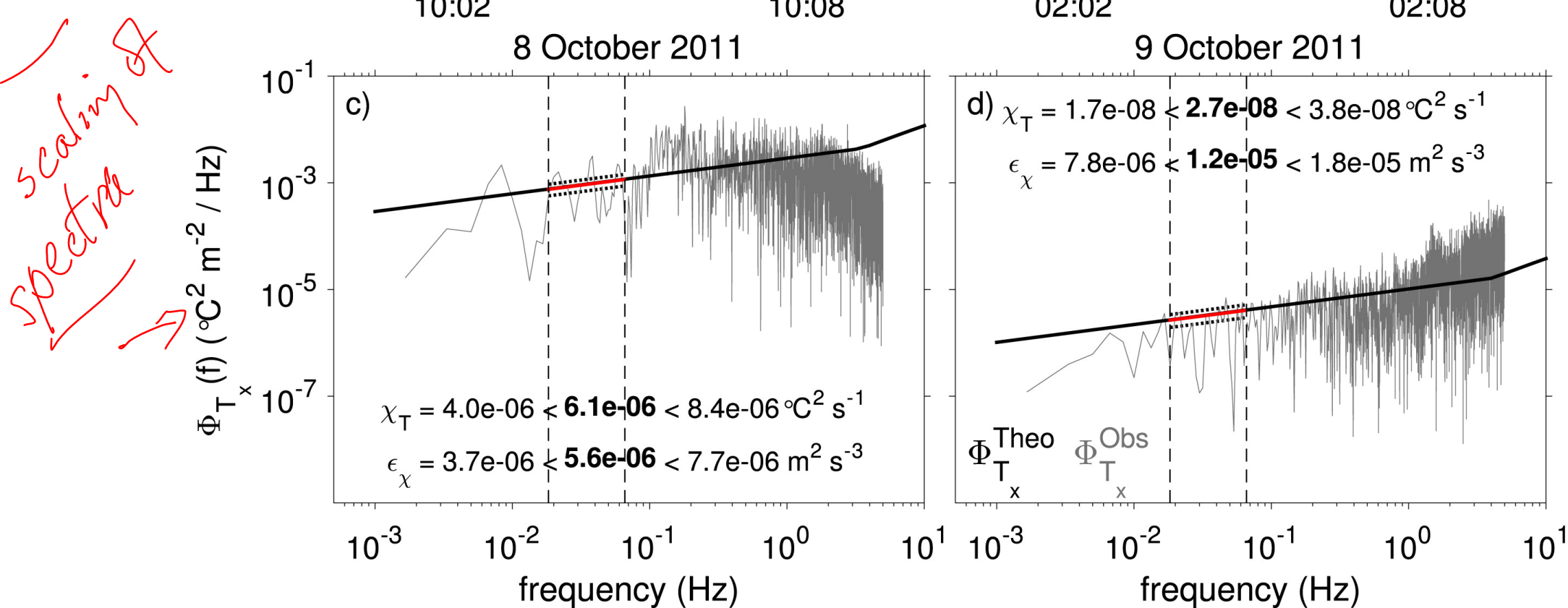
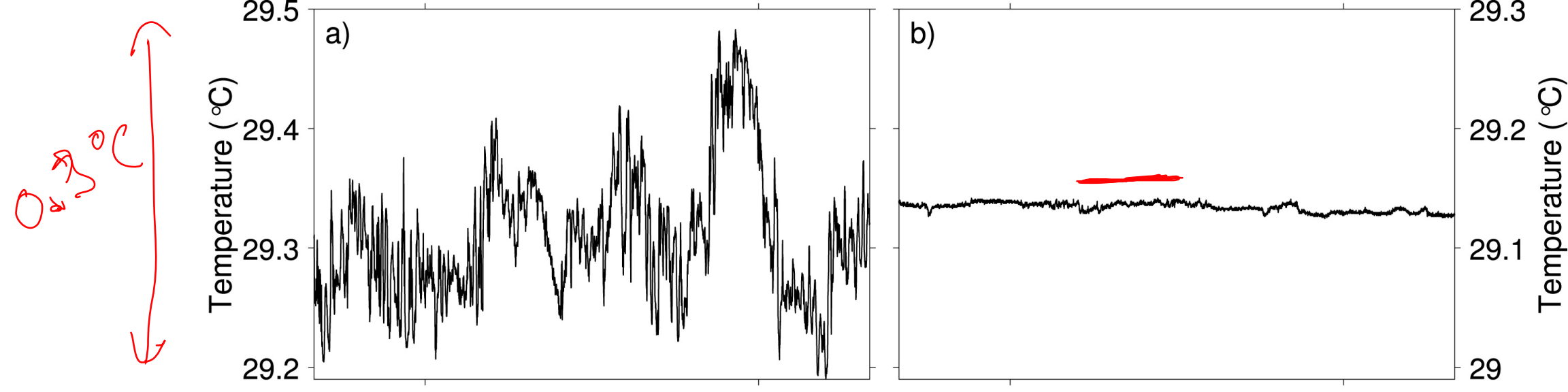


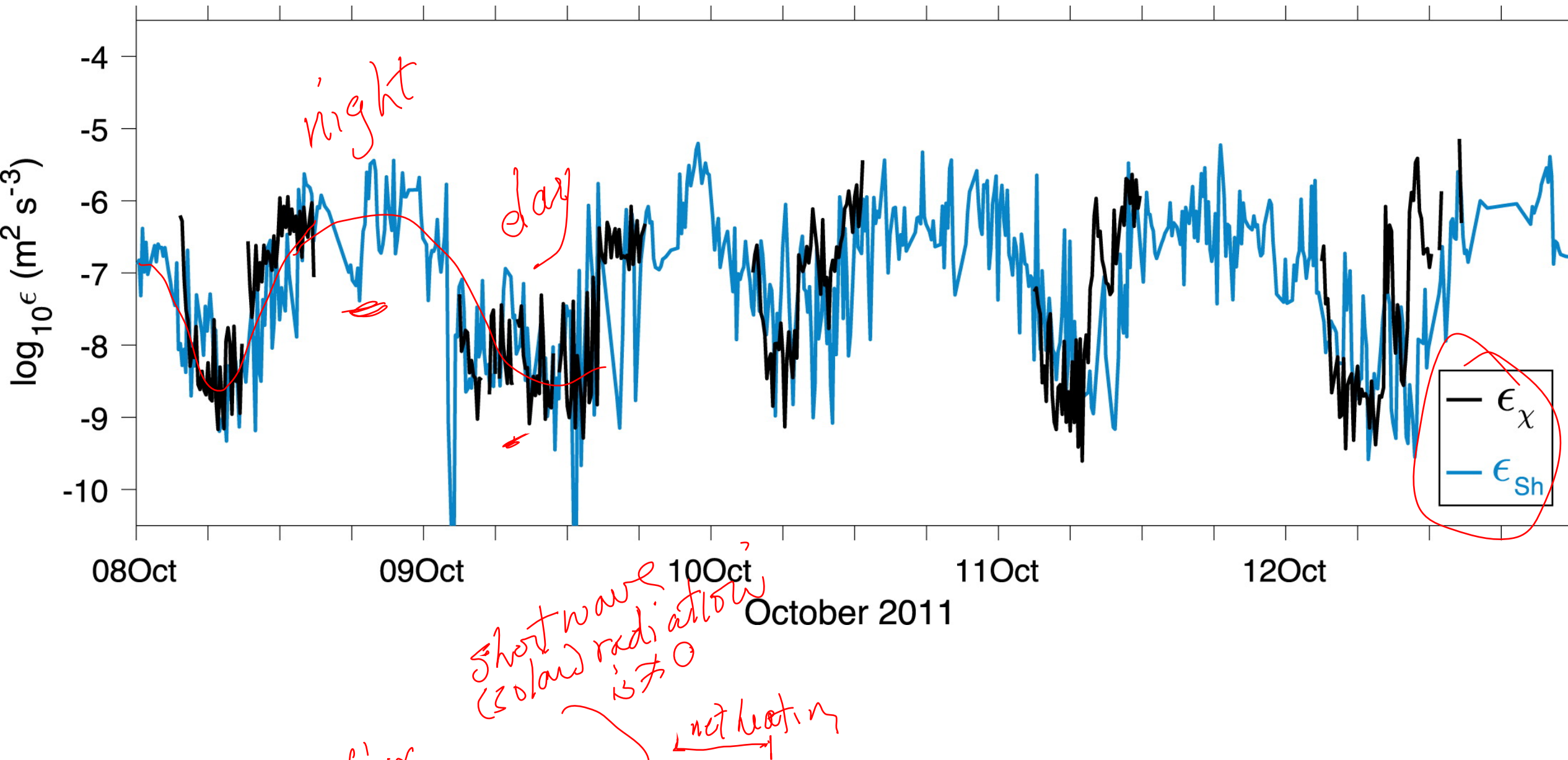
$\delta_1/\delta_2$  large, so is Shear  $\frac{\partial U}{\partial z}$

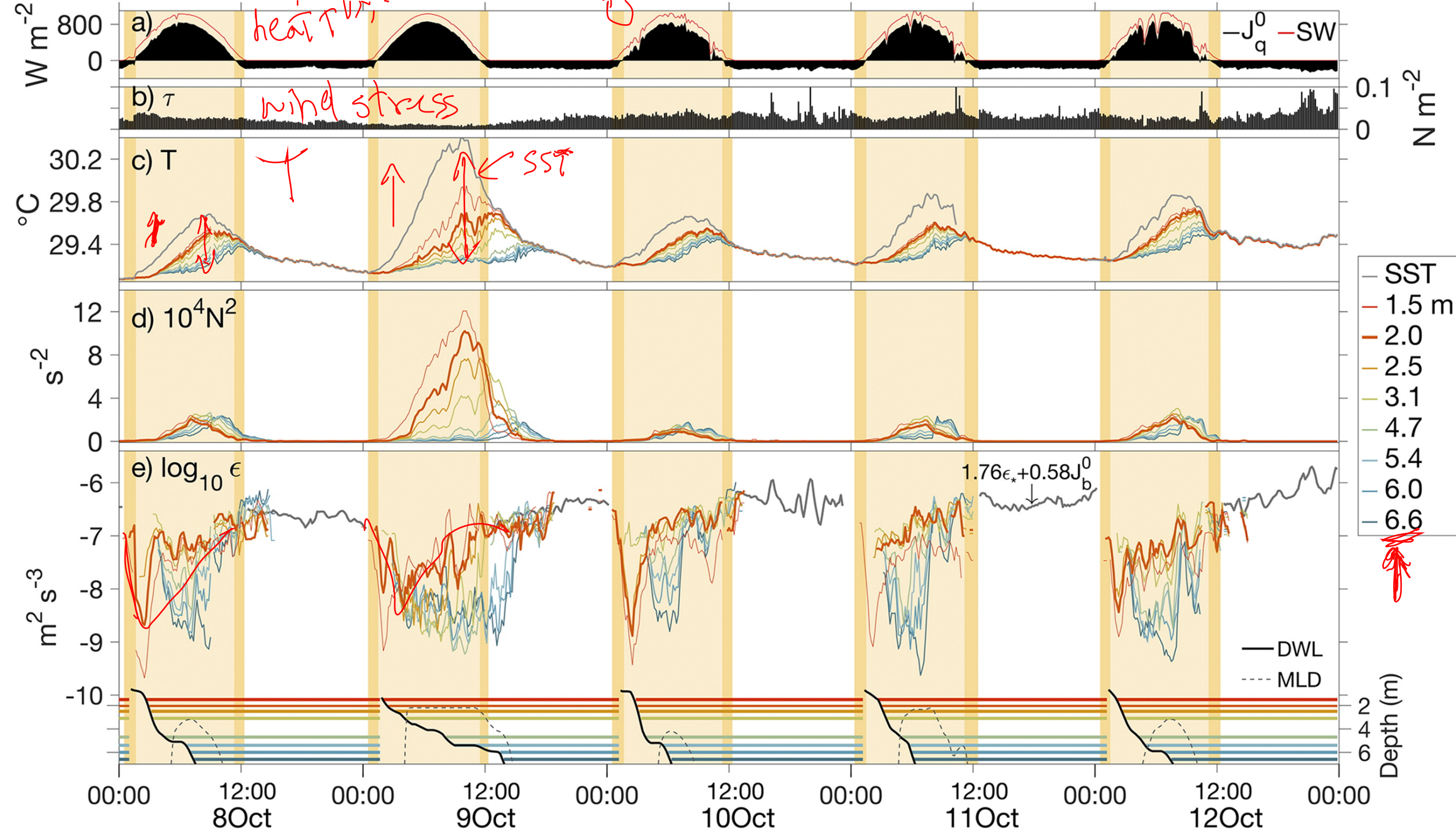


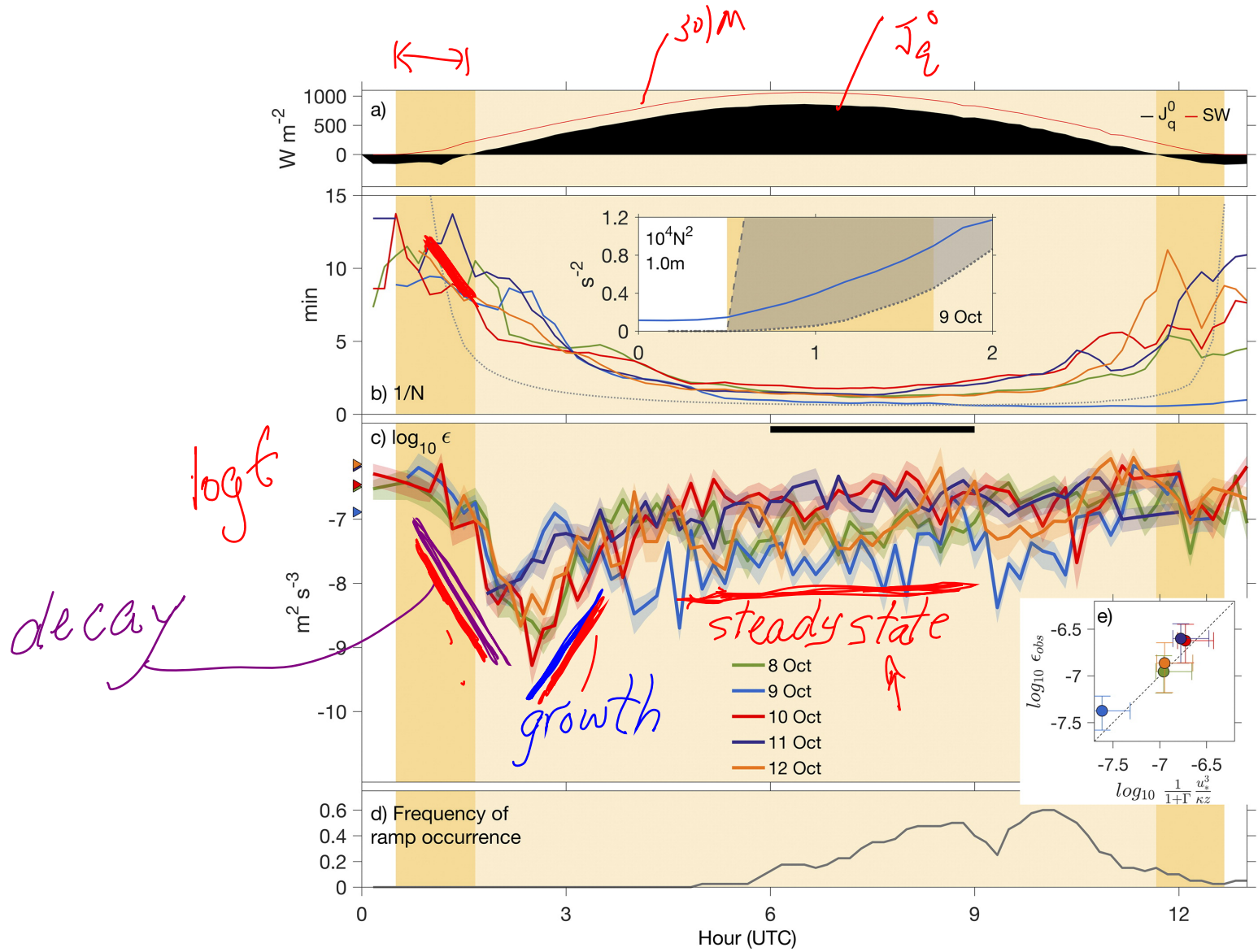
$\delta_1 + \delta_2 = \text{surface}$   $\left[ 2\theta_\alpha \quad 2\bar{T}_g \right]$









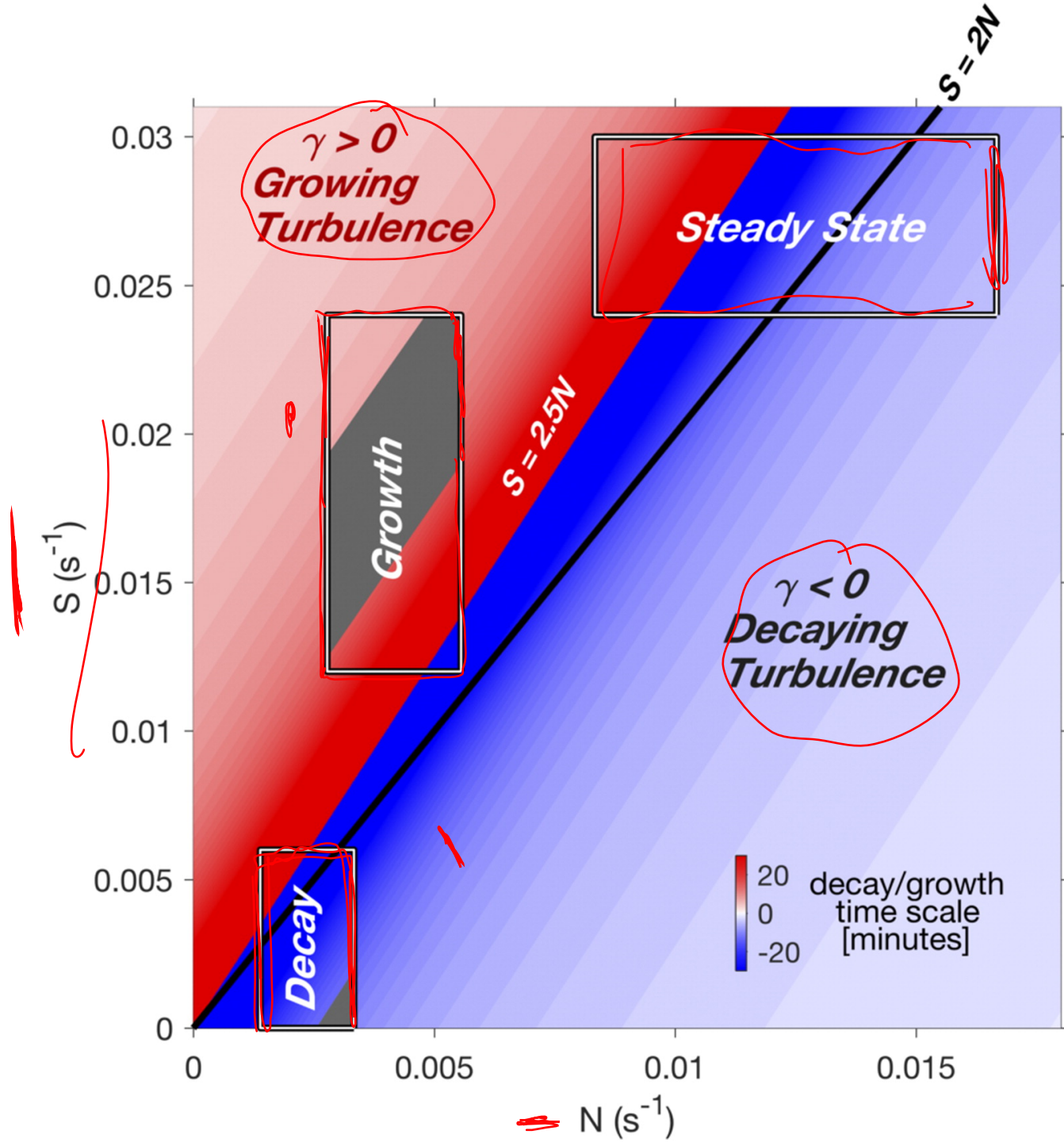


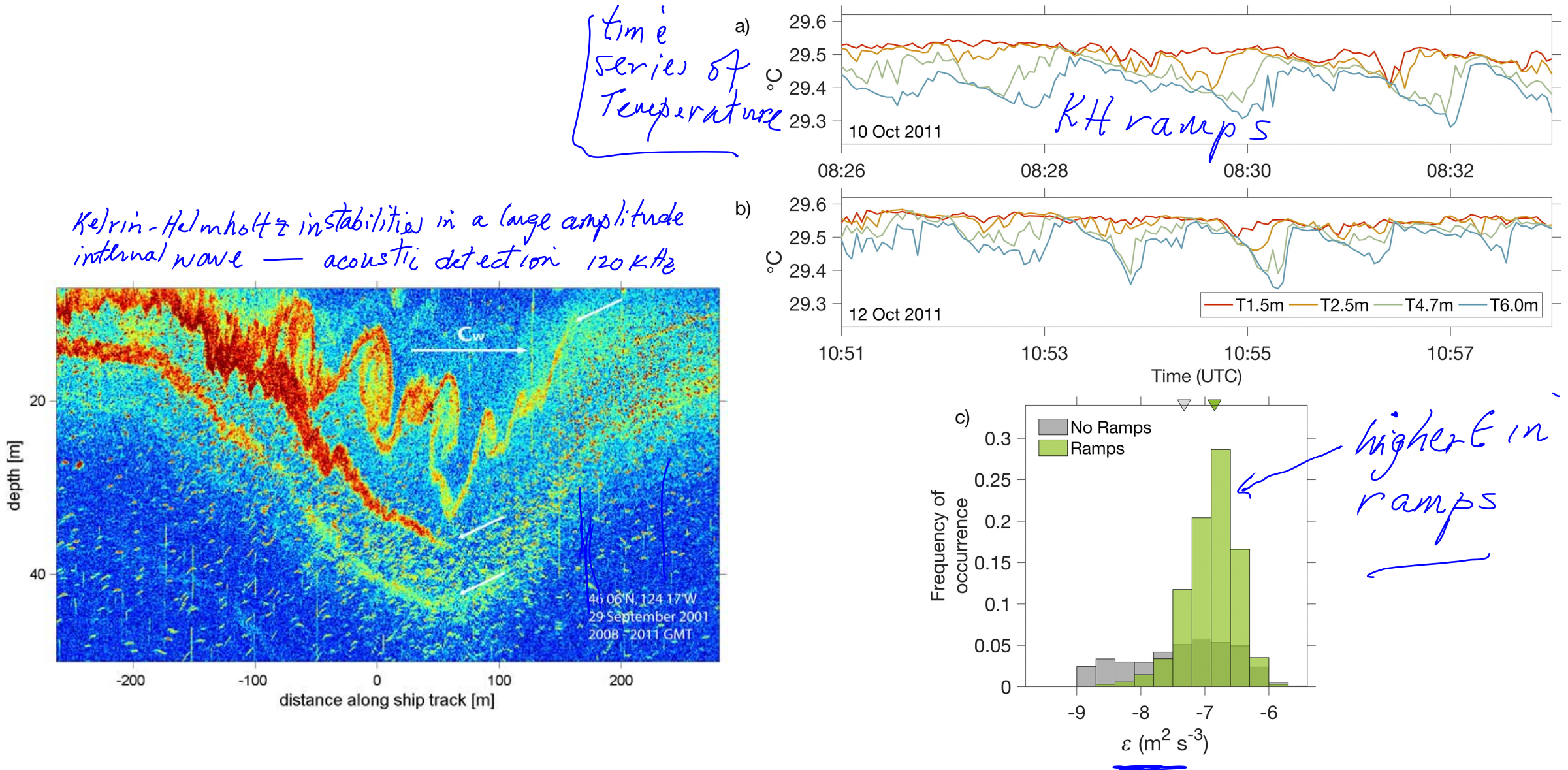
## **Evolution of Turbulence in the Diurnal Warm Layer**

Aurélie J. Moulin, James N. Moum, and Emily L. Shroyer

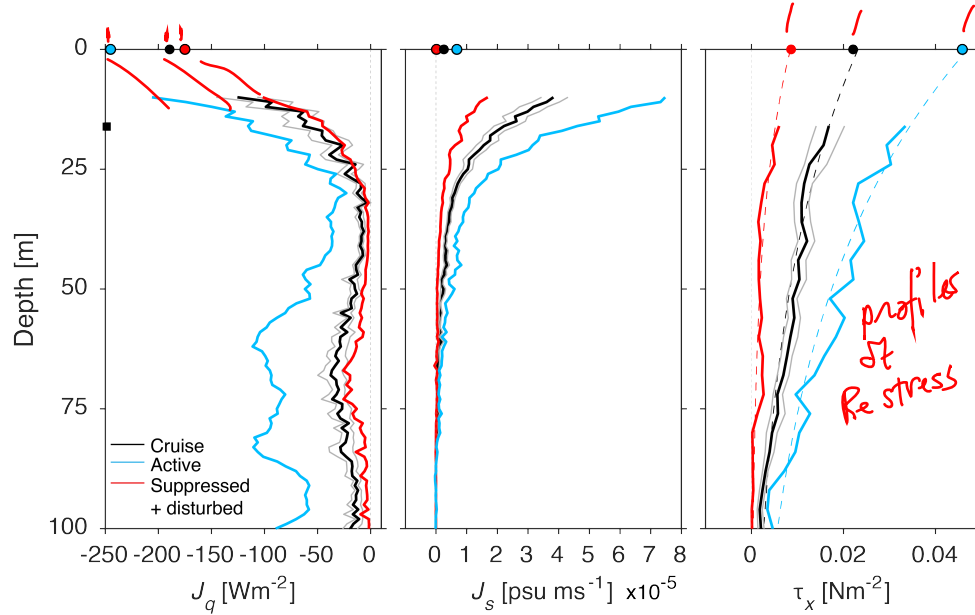
<https://journals.ametsoc.org/doi/full/10.1175/JPO-D-17-0170.1>

back to the whiteboard to  
develop new version of  
time-dependent tke equation  
→ lecture q.





## matching fluxes at the air-sea interface



Fluxes must be continuous.  
That is  
 $\frac{\partial \text{flux}}{\partial z}$  must be finite